



Consistent Initial Conditions for the Saint-Venant Equations in River Network Modeling

Cheng-Wei Yu

Center for Water and the Environment, The University of Texas at Austin

email: yuchanway@utexas.edu

Frank Liu

IBM Research Austin

email: frankliu@us.ibm.com

Ben R. Hodges

Center for Water and the Environment, The University of Texas at Austin

email: hodges@utexas.edu

Running head: Initial Conditions for Saint-Venant Equations

Abstract

1
2
3
4
5
6
7
8
9
10
11
12

Initial conditions for flows and depths (cross-sectional areas) throughout a river network are required for any time-marching (unsteady) solution of the one-dimensional (1D) hydrodynamic Saint-Venant equations. For a river network modeled with several Strahler orders of tributaries, comprehensive and consistent synoptic data are typically lacking and synthetic starting conditions are needed. Because of underlying nonlinearity, poorly-defined or inconsistent initial conditions can lead to convergence problems and long spin-up times in an unsteady solver. Two new approaches are defined and demonstrated herein for computing flows and cross-sectional areas (or depths). These methods can produce an initial condition data set that is consistent with modeled landscape runoff and river geometry boundary conditions at the initial time. These new methods are: (1) the Pseudo-Time-Marching Method (PTM) that iterates toward a steady-state initial condition using an unsteady Saint-Venant solver, and (2) the Steady-Solution Method



13 (SSM) that makes use of graph theory for initial flow rates and solution of a steady-state 1D
14 momentum equation for the channel cross-sectional areas. The PTM is shown to be adequate
15 for short river reaches, but is significantly slower and has occasional non-convergent behavior
16 for large river networks. The SSM approach is shown to provide rapid solution of consistent
17 initial conditions for both small and large networks, albeit with the requirement that additional
18 code must be written rather than applying an existing unsteady Saint-Venant solver.

19

20 Keywords: Flood modeling, One-dimensional models, River channels, Streams and rivers Initial
21 condition, Model spin up

22

23 **1 Introduction**

24 **1.1 Motivation**

25 Setting initial conditions for unsteady simulations of the Saint-Venant equations (SVE) across
26 large river networks can be challenging. Every element of the river network must be given
27 initial values of flow and depth, and these values should be consistent with the inflow boundary
28 conditions (e.g. from a land surface model) at the starting time to prevent instabilities. This
29 issue has not been previously addressed in the literature, arguably because it is essentially trivial
30 for the simple SVE systems that are usually modeled.

31 Saint-Venant equation modeling arguably dates from Priessmann's seminal work (Priess-
32 mann, 1961; Priessmann and Cunge, 1961), followed by decades of advances in techniques and
33 applications (Cunge, 1974; Ponce et al., 1978; Cunge et al., 1980; Abbott et al., 1986; Zhao
34 et al., 1996; Sanders, 2001; Pramanik et al., 2010). These models focused on hydraulics of short
35 river reaches or main stem rivers that are easy to initialize for flow and depth. It is only re-
36 cently that the solvers for large river networks have become practical (Hodges, 2013; Liu and
37 Hodges, 2014), and it is with large networks that the initial conditions are problematic. In-
38 deed, initial conditions and associated spin-up problems have been recently acknowledged and
39 investigated for hydrological models (e.g. Ajami et al., 2014), but without consideration of a
40 separate river network model. Work by Seck et al. (2015) and Rahman and Lu (2015) show that
41 hydrological model spin-up computational times could be significant and were dominated by the
42 selected initial hydrological conditions. (The spin-up time is the time it takes for the unsteady
43 time-marching model results to be insensitive to perturbations of the initial conditions).

44 Our experience with river network modeling is that simple approaches to initial conditions
45 often cause localized numerical instabilities, slow convergence of numerical solvers, and long
46 model spin-up times. Herein, we investigate the initial condition problem for a river network



47 model for a given set of inflows from a hydrological model.

48 **1.2 Consistency of initial conditions**

49 The “perfect” initial conditions with zero spin-up time would require flows and depths con-
50 sistent with (i) the actual unsteady behavior prior to the model start time and (ii) the model
51 boundary conditions – the latter includes both the bathymetric model for the river channels and
52 the coupled hydrological model providing runoff and base flows. However, such perfect initial
53 conditions are likely unattainable due to the sparsity of synoptic flow/depth data as well as
54 unavoidable uncertainty and errors in both bathymetric and hydrological models. A key point
55 is that the exact observed river initial conditions (if such were available throughout a network)
56 will *not* eliminate spin-up time if the observed data are inconsistent with the model boundary
57 conditions. Indeed, inconsistency between the river network model initial conditions and the
58 boundary conditions from a coupled hydrological model can lead to unrealistic impulses in time-
59 marching the SVE solution, which can destabilize a model. An extreme example is a high runoff
60 rate into an almost dry stream that can cause a Gibbs phenomenon at a wave front and negative
61 values for the computed cross-sectional area (Lax, 2006; Kvočka et al., 2015; Yang et al., 2012).
62 Although there are several models and studies claim that the numerical discontinuities can be
63 captured and resolved (Kazolea and Delis, 2013; Caleffi et al., 2003; Liang et al., 2006), the high
64 computational cost is still a burden for river models (Kvočka et al., 2015). We argue that the
65 primary goal of a set of synthetic initial conditions is providing consistency with the boundary
66 conditions to allow a smooth, convergent startup of an unsteady solver. Model spin-up time
67 is only completed when the river flows/depths are entirely determined by the flows from the
68 hydrological model, thus the observed flows/depths (which can slow the unsteady solver con-
69 vergence) are less valuable than a consistent set of flows/depths that provide a smooth starting
70 point.

71 **1.3 Initial condition approaches**

72 Approaches for specifying initial conditions for the SVE can be grouped into three main cate-
73 gories: (i) a “synoptic start” applying an interpolated/extrapolated set of sparse observational
74 data, (ii) a “cold start” with initial flow rates and flow depths prescribed either as zero (e.g.
75 Chau and Lee, 1991) or from some analytical values, e.g. mean annual flows and depths, and
76 (iii) a “steady-state” start, which we describe herein. The metric for evaluating initial condi-
77 tions is *not* how well they reflect available real-world observations, but how effective they are in
78 efficiently providing a consistent set of initial conditions.

79 As noted above, the first approach (synoptic start) is unlikely to be efficient for SVE ini-
80 tial conditions in a large river network due to inconsistencies between observations and model



81 boundary conditions as well as inconsistencies caused by interpolating/extrapolating sparse ob-
82 servations throughout a network. There are no proven approaches to analyzing consistency and
83 melding observations to hydrological model runoff, so the river network model spin-up will be
84 subject to random inconsistencies and instabilities that can delay or prevent convergence.

85 The second approach, a cold start, can provide smooth consistency over the river network
86 by using mean annual flows and depths (e.g. from the NHDplus data in the USA). Although
87 such cold start initial conditions are internally consistent, they may be far from the flows/depths
88 implied by the initial hydrological forcing. As a result, a cold start can require extensive spin-up
89 time to dilute or wash out the error. Using a cold start approach, the spin-up time dominated
90 the computational time for the large SVE networks we previously modeled in Liu and Hodges
91 (2014).

92 Herein we investigate the third approach, steady-state initial conditions, as a preferred for
93 initializing a large river network model. With this idea, a set of consistent initial conditions is one
94 that satisfies both the $t = 0$ hydrological forcing and the *steady-state* Saint-Venant equations
95 at $t = 0$. Although a river system is unlikely to be steady-state, we argue that the initial
96 conditions are always a compromise and the end goal is to reduce the spin-up time rather than
97 match reality. This approach has the advantage of providing flows and depths that are consistent
98 across the entire network with all the boundary conditions (inflows and channel geometry) as
99 well as the nonlinear governing equations. This consistency eliminates destabilizing impulses
100 otherwise caused by mismatches between the flow/depth in a river reach and the runoff, so
101 subsequent time-marching of the unsteady solution is smooth. This approach can dramatically
102 reduce the subsequent spin-up time for the unsteady solution.

103 1.4 Overview

104 Herein we present an efficient approach to establishing a set of steady-state conditions that
105 provides a consistent and smooth starting point for time-marching an unsteady Saint-Venant
106 simulation. A full model initialization problem has two parts: (i) determine a set of flows and
107 water surface elevations that are consistent steady solutions of the SVE for starting an unsteady
108 solver, and (ii) determine the spin-up time needed to ensure error in the initial conditions are
109 washed out of the unsteady solution. The second problem is highly dependent on the network
110 characteristics and the particular flow and boundary conditions during spin-up, so for brevity,
111 this work deals quantitatively with solving the first problem, and then illustrates the effects on
112 the second problem.



2 Methods

2.1 Saint-Venant equations

The Saint-Venant equations for temporal (t) evolution of flow and water surface elevation along one spatial dimension (x) following a river channel are generally derived using the hydrostatic and Boussinesq approximations applied to the incompressible Navier-Stokes and continuity equations. Cross-section averaging to obtain the 1D equations is considered reasonable where cross-sectional gradients are smaller than along-channel gradients. However, the equations are widely used even where such assumptions are questionable (e.g. near a bridge with multiple immersed piers), with the effects of significant cross-section gradients or non-hydrostatic behavior being represented as empirical energy losses. A number of conservative and non-conservative equation forms have been used, with different advantages and disadvantages (Hodges and Liu, 2014). Herein we follow Liu and Hodges (2014) in using cross-sectional area (A) and flow rate (Q) as principle solution variables of the numerical system and the local water depth (h) and friction slope (S_f) as a secondary variables (i.e. variables that depend on A and Q through auxiliary relationships). The equation set can be written as:

$$\frac{\partial A}{\partial t} + \frac{\partial Q}{\partial x} = q_t \quad (1)$$

$$\frac{\partial Q}{\partial t} + \frac{\partial}{\partial x} \left(\frac{Q^2}{A} \right) + gA \frac{\partial h}{\partial x} = gA(S_0 - S_f) \quad (2)$$

where boundary conditions are the local channel bottom slope (S_0) and the local lateral net inflow (q_t), the latter representing both inflows from the landscape and outflows to groundwater. Auxiliary equations for $h = h(A)$ are derived from river cross-section data. The Chezy-Manning equation can be used to provide the friction slope as:

$$AS_f = \tilde{n}^2 Q^2 F \quad (3)$$

where \tilde{n} is the standard Manning's n roughness coefficient and F is a convenient equivalent friction geometry (Liu and Hodges, 2014), which subsumes the conventional hydraulic radius (R_h) using a definition of

$$F = \frac{1}{AR_h^{4/3}} = \left(\frac{P^4}{A^7} \right)^{1/3} \quad (4)$$

with $P = P(A)$ is the wetted perimeter and $R_h = AP^{-1}$. Note that eq. (4) fixes a typographical error in eq. (10) of Liu and Hodges (2014) and eq. (3.55) of Hodges and Liu (2014). Required boundary conditions for the unsteady Saint-Venant solution are $q_t(t)$ for each stream



138 segment, $Q_{bc}(t)$ at the furthest upstream node (headwater) in river branches with a Strahler
139 order of one, and h with an $h(A)$ relationship at the downstream boundary (assumed subcriti-
140 cal). The time-marching unsteady solution requires initial conditions for (Q, A) , which can also
141 be given as (Q, h) with $A = A(h)$. Implementation details of the unsteady solver used herein
142 can be found in Liu and Hodges (2014) and Liu (2014).

143 2.2 Pseudo time-marching approach

144 The most obvious approach for finding steady-state initial conditions is to time-march an un-
145 steady solver until a steady state is achieved. That is, we apply the unsteady solver with
146 time-invariant boundary conditions of $q_l(t) = q_l(0)$ and $Q_{bc}(t) = Q_{bc}(0)$ for $t_0 \leq t < 0$ where
147 t_0 is our pseudo-time start and $t = 0$ is the time for which we want a set of initial conditions.
148 We call this the “pseudo time-marching method” (PTM). The initial condition for PTM is a set
149 of $Q(t_0)$ and $A(t_0)$ for each stream segment (e.g. cold start conditions as described above). At
150 first glance, the logic here might seem circular: we are trying to solve for initial condition set
151 $\{Q(0), A(0)\}$ of the unsteady model and PTM requires specifying $\{Q(t_0), A(t_0)\}$. This begs the
152 question as to why PTM should be used rather than simply apply a cold start of the unsteady
153 solver with $Q(0) = Q(t_0)$ and $A(0) = A(t_0)$. The answer is that the key difference between the
154 PTM using $Q(t_0)$ and $A(t_0)$ and a cold start of the unsteady solver with the same values is that
155 the former has time-invariant boundary conditions while the latter’s are time-varying. Thus, an
156 unsteady solver with time-varying boundary conditions is trying to take an inconsistent start-
157 ing condition and converge it to a moving target. In contrast, the PTM takes the inconsistent
158 starting conditions and attempts to converge them to a time-invariant target, which is more
159 likely to be successful.

160 The PTM is outlined as Algorithm 1. A user-selected parameter (ϵ) is used as a threshold
161 tolerance value for declaring convergence to the steady state. A typical choice of the tolerance ϵ is
162 the square root of the computer hardware tolerance. For example, on a 64-bit Intel architecture,
163 the hardware tolerance for a double precision floating point floating number is 2.2204×10^{-16} ,
164 which means a good choice of ϵ is 1.4901×10^{-8} . As a practical matter, ϵ of 10^{-6} or even 10^{-4}
165 is likely to be sufficient for initial conditions; that is, as further spin-up time is still required to
166 dilute initial condition errors the convergence needs only to be sufficient for consistency across
167 the network. The method can use a time-step size that is either constant or varying, with an
168 automatic reduction in step size when convergence is not achieved in a given time step (Liu and
169 Hodges, 2014). To avoid infinite runtimes for non-convergent behavior (e.g. due to instabilities
170 developed with inconsistent starting conditions), the solution is terminated (failure to converge)
171 in Algorithm 1 after a user-selected N_{max} iterations. The starting conditions for $\{Q(t_0), A(t_0)\}$
172 are discussed in Appendix A.



Algorithm 1 Pseudo Time-Marching Method

1: **procedure** PSEUDOTIMEMARCHING(A_{ini} , Q_{ini} , ϵ , N_{max}) ▷ A_{ini}, Q_{ini} : initial guesses of A
and Q ; ϵ : tolerance; N_{max} : maximal iteration number

2: $A \leftarrow A_{ini}$

3: $Q \leftarrow Q_{ini}$

4: $i \leftarrow 0$

5: $t_0 \leftarrow 0$

6: **for** $i = 1$ to N_{max} **do**

7: Solve SVE at time point t_i using unsteady method

8: Compute error: $e \leftarrow |Q_t - Q_{t-1}| + |A_t - A_{t-1}|$

9: **if** $e < \epsilon$ **then**

10: **return** *Success*

11: **end if**

12: $t_{i+1} \leftarrow t_i + \Delta t_i$

13: $i \leftarrow i + 1$

14: **end for**

15: **return** *Failure*

16: **end procedure**



2.3 Steady-solution method

The PTM approach (above) results in a steady solution of the unsteady Saint-Venant equations that satisfies both momentum and continuity for time-invariant $q_l(0)$ and $Q_{bc}(0)$ boundary conditions in the unsteady solver. However, we can achieve a similar effect more directly by writing a steady-state version of the Saint-Venant equations as:

$$\frac{\partial Q}{\partial x} = q_l \quad (5)$$

$$\frac{\partial}{\partial x} \left(\frac{Q^2}{A} \right) + gA \frac{\partial h}{\partial x} = gA(S_0 - S_f) \quad (6)$$

A key point, implied by eq. (5), is that the spatial gradient of steady-state Q over a stream segment is entirely due to the lateral inflow (q_l) without any influence of A . It follows that for steady q_l and Q_{bc} boundary conditions, the flow in the i^{th} river segment (Q_i) that has Strahler order S_i must be the sum of all the Q_j for all the j connected reaches of Strahler order $S_j < S_i$. That is, the steady flow at any point is simply the sum of all the upstream $t = 0$ boundary conditions. Thus, the steady-state Q can be obtained (without solving a PDE) through a simple graph traversal technique. The corresponding A (and hence depth h) can then be computed with a numerical PDE solution of eq. (6). Note that for large river networks, the natural downstream boundary condition is subcritical, which requires specification of h and the corresponding A as the starting point. We call this a “steady-solution method” (SSM).

For river networks with simple junctions, such as Fig. 1, the flow direction in each segment is known *a priori* and the network corresponds to a “direct acyclic graph”, or DAG, in graph theory (Hodges and Liu, 2014). Although DAG systems allow both upstream and downstream splitting (e.g. two paths around an island), it does not allow flow directions that create a recirculating loop, which is consistent with water flow that cannot loop around to return to an upstream point. The connectivity of a DAG can be efficiently computed by applying existing graph methods, such as depth-first-search (DFS) or breadth-first-search (BFS), which provide simple and efficient approaches to computing $Q(0)$ for each stream segment over an entire network. Note that these methods were designed and named by computer scientists, so “depth” in DFS and “breadth” in BFS do not refer to hydraulics or river geometry, but instead are jargon referring to the graph network characteristics.

A DFS traversal (Cormen et al., 2001) for Q is shown in Algorithm 2. From each headwater node, the inflow boundary condition is propagated downstream by adding the value to the downstream node and including any lateral q_l . For river networks, the DFS traversal is highly efficient and requires negligible computational time for river networks of 10^5 computational nodes (e.g. Liu and Hodges, 2014). Based on our experience, the DFS computational costs should be essentially trivial for even continental-scale systems of 10^7 nodes.

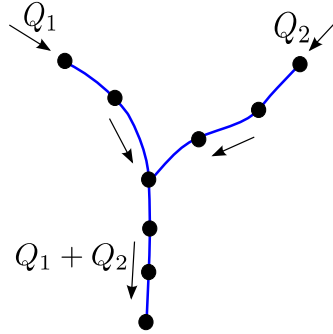


Figure 1: Propagation of flow rate Q at a junction.

205 After the steady Q_i for each stream segment is computed, eq. (6) can be solved for the
 206 corresponding A_i . We discretize this equation with the Preissmann scheme, similar to the
 207 approach used for the unsteady Saint-Venant equation in Liu and Hodges (2014). The value
 208 and derivative for any term are approximated as:

$$f(x, t) \simeq \frac{1}{2}(f_{j+1} + f_j) \quad (7)$$

$$\frac{\partial}{\partial x} f(x, t) \simeq \frac{1}{\Delta x}(f_{j+1} - f_j) \quad (8)$$

209 where subscripts indicate a node in the discrete system. Using $j + 1/2$ to represent geometric
 210 data that is logically between nodes (i.e. roughness \tilde{n} and S_0), eq. (6) becomes:

$$\begin{aligned} & \frac{2}{\Delta x} \left[\frac{(Q_{j+1})^2}{A_{j+1}} - \frac{(Q_j)^2}{A_j} \right] \\ & + \frac{g}{\Delta x} (A_{j+1} + A_j) (h_{j+1} - h_j) - g [A_{j+1} + A_j] S_{0(j+1/2)} \\ & + g \tilde{n}_{j+1/2}^2 \left[(Q_{j+1})^2 F_{j+1} + (Q_j)^2 F_j \right] = 0 \end{aligned} \quad (9)$$

211 These nonlinear equations are similar to the unsteady discrete equations, except that Q for each
 212 computational node is known from the DFS traversal. Newton's method is used to solve this
 213 system for A without linearization, similar to the approach in Liu and Hodges (2014). The SSM
 214 requires a starting guess for A to solve the steady-state problem. Herein we use a bisection
 215 method with the Chezy-Manning equation for normal depth conditions, discussed in Appendix
 216 A. The overall algorithm for SSM is illustrated in Algorithm 3.



Algorithm 2 DFS traversal for Q

```
1: procedure QTRAVERSAL
2:   for all  $i$  do                                     ▷ initialization
3:      $Q_i \leftarrow 0$ 
4:   end for
5:   for each headwater node  $j$  with BC  $Q_j(t)$  do
6:      $Q_j \leftarrow Q_j(t = 0)$ 
7:      $k \leftarrow$  downstream node of node  $j$ 
8:     while  $k$  is not empty do
9:        $Q_k \leftarrow Q_k + Q_j(t = 0)$ 
10:       $k \leftarrow$  downstream node of node  $k$ 
11:    end while
12:  end for
13:  return
14: end procedure
```

Algorithm 3 Steady-Solution Method

```
1: procedure STEADYSOLUTION
2:   Call QTraversal()
3:   for all node  $j$  in network do                       ▷ Initial guess of  $A$ 
4:     Call bisection routine BiSection( $Q_j$ )
5:   end for
6:   Solve steady version of dynamic eqn in eq. (9)
7:   return
8: end procedure
```



3 Computational Tests

3.1 Overview

The performance of PTM and SSM are examined with a series of test cases ranging from simple uniform cross-sections over short river reaches to 15,000 km of a real river network. To demonstrate the robustness and performance of the SSM, we conduct tests from three perspectives: (i) effects of different cross-section geometries; (ii) scalability with an increasing number of computational nodes; and (iii) real-world river networks. Two different computers are used: the cross-section and scalability tests are run on a computer with 2.00GHz Intel Xeon D-1540 CPU's and 64GB of RAM, while the large network tests are run on a computer with 2.52GHz Intel i7-870 CPU's and 8GB of RAM. In both cases Ubuntu Linux is the operating system and GNU C++ compiler is used.

3.2 Effects of cross-section geometry

Test cases for cross-section geometry effects were conducted for synthetic geometry of simple river reaches without tributaries. Cases included rectangular, parabolic, trapezoidal, and non-uniform cross-sections, with a range of channel lengths, widths, and computational nodes, as provided in Table 1.

test case	channel length (km)	number of computational nodes	cross-section shape type	cross-section shape detail
Case 1	3.1	78	Uniform rectangular	$W_B = 20$ m
Case 2	0.2	6	Uniform trapezoidal	$W_B = 1$ m $S_{sw} = 0.5$
Case 3	0.3	6	Uniform trapezoidal	$W_B = 0.1$ m $S_{sw} = 1.5$
Case 4	5.6	71	Uniform trapezoidal	$W_B = 10$ m $S_{sw} = 0.5$
Case 5	10	167	Uniform quasi-parabolic	$f = 37.8$
Case 6	10	1664	Surveyed bathymetry	Unsymmetrical cross-section
Case 7	122	31	Surveyed bathymetry	Unsymmetrical cross-section

Table 1: Cross-section geometry test cases. W_B and S_{sw} represent bottom width and sidewall slope respectively, f represents the focal length of parabolic shape.

3.3 Scalability

To demonstrate the scalability as the number of computational nodes increases, we use the geometry and flow conditions of Case 4 in Table 1 and generate synthetic test cases with increasing



236 numbers of nodes from a few hundred to over a million in the set: { 560, 2800, 5600, 11200,
237 22400, 44800, 89600, 179200, 358400, 716800, 1433600 }.

238 3.4 Large river networks

239 To examine the robustness of PTM and SSM for more realistic conditions over both small and
240 large scales, we use a section of Waller Creek (Texas, USA) as well as the entire watershed of the
241 San Antonio and Guadalupe River basins (Texas, USA). The former is a small urban watershed
242 for which dense cross-section survey data is available, whereas the latter is a large river basin
243 that has been previously modeled with the RAPID Muskingum routing model (David et al.,
244 2011) and the SPRNT Saint-Venant model (Liu and Hodges, 2014).

245 The Waller Creek study includes two stream reaches and the catchment area illustrated in
246 Fig. 2. The total stream length is 11.6 km, which drains an area of 14.3 km². The layout of
247 Waller Creek is shown in Fig 2(a), and parts of the bathymetry surveyed data from City of
248 Austin is shown in Fig. 2(b) for clarity. Two different model geometries were considered, which
249 are designated as *WCA* and *WCB*. For *WCA* the stream is discretized by 373 computational
250 nodes based on separation of the surveyed cross-sections. *WCA* neglects the minor tributary of
251 Waller Creek and includes the full complexity of the surveyed cross-sections shown in Fig. 2(b).
252 In contrast, *WCB* includes both tributaries, but uses wider computational node separation with
253 only 30 of the 373 surveyed cross-sections.

254 To test the initial condition approach for a large river network, we use the San Antonio
255 and Guadalupe River basins (Fig. 3), which have a combined total stream length of 12,728
256 km (excluding some minor first-order segments). The model herein uses 63,777 computational
257 nodes, 59,594 segments, and 2,643 junctions, but is otherwise similar to the model setup with
258 1.3×10^5 nodes used in Liu and Hodges (2014). Although the unsteady SPRNT model is
259 typically run by coupling with a land-surface model for headwater and lateral inflows, for the
260 present steady-state tests we used a synthetic inflow data set for the headwater inflows. The
261 synthetic flow at each headwater stream was computed based on a downstream peak flow rate
262 distributed uniformly across all the headwater reaches. We used the peak flow rate recorded on
263 the main stem of Guadalupe River at Victoria (Texas) on January 19th, 2010 by USGS gauge
264 08176500. As this gauge does not include the San Antonio River flows, we divided the peak flow
265 rate ($453 \text{ m}^3\text{s}^{-1}$) by the total number of headwater streams in the Guadalupe River (815) to
266 get a single inflow value that was applied to each headwater reach ($0.55 \text{ m}^3\text{s}^{-1}$). The same flow
267 rate was used for the 725 headwater reaches of the San Antonio River network. This approach
268 ensures that there is flow in every branch in the river network.

269 Following Liu and Hodges (2014), it is necessary to estimate the cross-section geometry for this
270 river network as comprehensive survey data are not available. Because the geometry affects

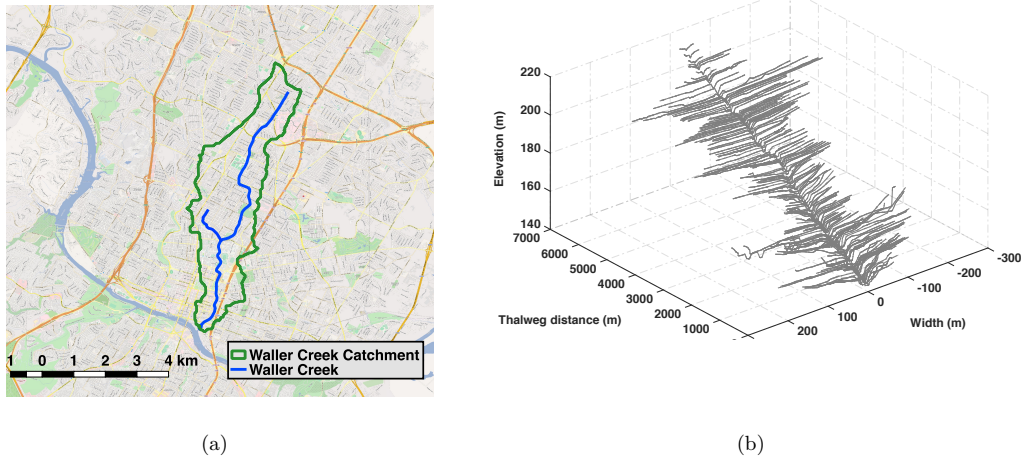


Figure 2: (a) Waller Creek and catchment in Austin (Texas, USA) (b) Surveyed cross-sections of main channel for Waller Creek (Texas). Only 149 of 327 cross-sections are shown for clarity. Elevations are relative to mean sea level. Data courtesy of City of Austin.

271 both PTM and SSM solutions, we tested four different estimation approaches (Cases *A*, *B*,
 272 *C*, and *D*). Cases *A* uses synthetic trapezoidal cross-sections using the approach applied in
 273 Liu and Hodges (2014) based on Western et al. (1997). In this method, trapezoidal widths
 274 (W) are computed from mean annual flows (Q_m) from the NHDPlus dataset as $W = \alpha Q_m^{0.5}$
 275 with $\alpha = 1.5$. For the side slope of trapezoidal cross section, an identical sidewall slope (45
 276 degrees) is used throughout the river network. Case *B* channels were similar to Case *A*, but
 277 included some minor changes to Manning’s n , inflow boundary conditions, and channel bottom
 278 slopes in reaches where instabilities occurred, which was necessary to provide convergence for
 279 the PTM (see §4.5). Case *C* channels were based on work of Santibanez (2015), who used USGS
 280 streamflow measurements in the San Antonio and Guadalupe River network along with the at-
 281 a-station hydraulic geometry approach (Rhodes, 1977) to find the best trapezoidal cross-section
 282 approximation for the drainage area. Using this approach, the bed width (b_0) is an exponential
 283 function of cumulative drainage area (A_D) as:

$$b_0 = \gamma A_D^\lambda \quad (10)$$

284 where b_0 is meters, A_D is km^2 , and the coefficients are $\gamma = 12.59$ and $\lambda = 0.382$. The Santibanez
 285 (2015) approach provides reasonable values for trapezoidal channel sidewall slopes over most of
 286 the basin, but fails in many of the first-order streams with small drainage areas ($< 25 \text{ km}^2$)



287 where the computed sidewall slopes are near zero. For simplicity in the present test cases, a
288 uniform value of 45 degrees is used for the sidewall slopes throughout the river network. Case *D*
289 uses channel bathymetry data generated from Zheng (2016), which uses a Height Above Nearest
290 Drainage (HAND) analysis (Nobre et al., 2011) applied to the National Elevation Dataset (NED)
291 to provide an automated approach for estimating trapezoid-based composite cross-sections.

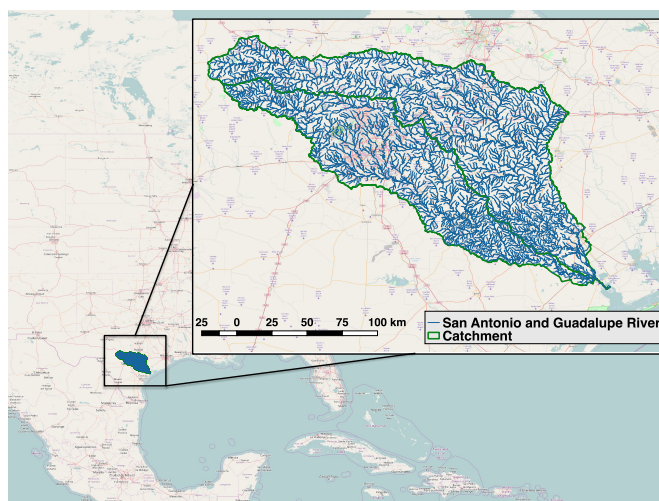


Figure 3: San Antonio and Guadalupe River network, from NHDPlus V2 Flowline



4 Results

4.1 Comparison metrics

The overall algorithm efficiency is evaluated by the number of Newton iterations required for convergence to steady-state. The number of Newton iterations reflects the difficulty in converging the nonlinear solution and is proportional to the simulation runtime. As this metric is independent of computer architecture it provides a universal measure of algorithm performance. For SSM we use the number of iterations to converge the A solution, which is the dominant computational cost (i.e. the non-iterative graph-traversal solution for Q is negligible in comparison). For PTM, we use the cumulative sum of Newton iterations for the (Q, A) solution over all pseudo-time steps. Where converged solutions of PTM and SSM both exist, comparisons (not shown) indicate the resulting (Q, A) steady-state results are identical within the convergence tolerance ($\epsilon = 10^{-6}$).

4.2 Effects of cross-section geometry

Table 2 provides a comparison of Newton iterations for the test cases of Table 1 for single reaches with different channel cross-sections. The SSM converges quickly across all cases, whereas the performance of the PTM is always substantially slower than the SSM. The performance of the PTM appears somewhat erratic, which is likely because the overall number of pseudo-time steps depends on how far the starting guess is from the converged answer and the size of the time step used in the PTM pseudo time march. The SSM approach is always faster, arguably because the update magnitude in each Newton iteration is not limited by a time step size.

test case	PTM iterations	SSM iterations	relative speed-up of SSM
Case 1	327	6	54×
Case 2	73	4	18×
Case 3	136	8	17×
Case 4	773	9	85×
Case 5	8634	76	113×
Case 6	13 765	4	3441×
Case 7	91 234	30	3041×

Table 2: Newton iterations required to achieve convergence for benchmark geometry test cases. The converged results are identical for both methods.

By comparing the geometric data from Table 1 with the results in Table 2, it can be seen



313 that the largest discrepancies between PTM and SSM performance (Cases 6, 7) are with non-
314 uniform cross-sections. In both of these the SSM performs $O(10^3)$ times better, compared to
315 $O(10)$ to $O(10^2)$ improvements for simple geometry. This result is consistent with the idea
316 that the performance of PTM depends on how close the starting guess for $\{Q, A\}$ is to the
317 steady-state solution. With non-uniform cross-section geometry, the starting guess is generally
318 a quite far from the steady-state condition as it is difficult to *a priori* estimate gradients of
319 the water surface that match the nonlinear acceleration associated with cross-section variability.
320 In contrast, the benchmark tests with simple cross-section geometry (Cases 1-5) show more
321 modest speed-up by SSM, which is consistent with the steady-state solution for PTM with
322 simple geometry being closer to the starting guess. For short reaches with simple geometry and
323 only a few computational nodes (Case 2, 3) the speed-up by SSM is essentially irrelevant.

324 4.3 Scalability

325 Computing initial conditions using models with varying numbers of computational nodes for
326 Case 4 in Table 1 provides the speed-up results shown in Fig. 4. These tests use simple trape-
327 zoidal cross-sections and, consistent with the results above, the speed-up advantage of the SSM
328 is relatively modest with less than 10^3 nodes. However, beyond this point, the effective speed-up
329 with SSM is quite dramatic. It appears that the SSM method becomes more effective than PTM
330 both with increasing complexity of the cross-sectional geometry and the increasing number of
331 computational nodes.

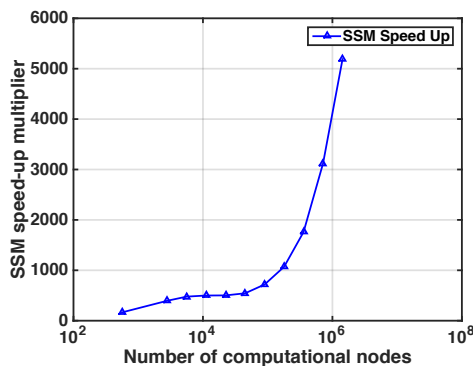


Figure 4: Speed-up multiplier of SSM compared to PTM for Case 4 as a function of the number of computational nodes.



332 **4.4 Waller Creek test cases**

333 The results of initial condition convergence for two Waller Creek simulations are shown in
334 Table 3. The SSM method dramatically reduces the total number of iteration to convergence,
335 which is also reflected in reducing the computer runtime by 99% and 92% for *WCA* and *WCB*,
336 respectively. Although the absolute runtime for this small system is trivial by either PTM
337 or SSM, the disparity provides insight into the performance that is confirmed with the more
338 complicated river network, discussed below.

configuration	pseudo time-marching iterations (PTM)	steady-solution iterations (SSM)	relative speed-up of SSM	PTM runtime	SSM runtime
<i>WCA</i>	2900	23	130×	1.570 sec	0.011 sec
<i>WCB</i>	890	13	70×	0.037 sec	0.003 sec

Table 3: Total Newton's iterations required to achieve convergence of the Waller Creek Creek test case.



4.5 San Antonio and Guadalupe River basins

The results of the full river network computations are provided in Table 4, which shows the SSM was successful and used a relatively small number of Newton iterations despite the complexity of the system. However, three of the PTM solutions could not be stabilized; that is, the method diverged from any selected starting condition and finally caused convergence failure. Indeed, it was the inability to converge PTM with configurations *A*, *C*, and *D* that led to the development of configuration *B* as a modification of *A*. To obtain the geometry for *B*, we identified reaches where instabilities developed in PTM and made minor ad hoc adjustments for Manning’s *n*, inflow boundary conditions, and channel bottom slopes until we achieved convergence. Note that the modeler’s time to tune the system for the PTM method to successfully converge is not included in the comparisons of Table 4.

The convergence behavior of the PTM is shown in Fig. 5. It can be seen that for several hundred time marching steps the solution was oscillating rather dramatically, but eventually settled down to a slow, smooth behavior. We believe this is evidence of the PTM trying to overcome inconsistencies between the $\{Q(t_0), A(t_0)\}$ starting conditions and the time-invariant boundary conditions in the network. Note that PTM for *B* was not converged to the same $\epsilon = 10^{-6}$ tolerance used for SSM. Instead, the solution was manually terminated after 9+ hours, when the convergence norm reached 1.6×10^{-4} and was sufficiently smooth so that it was clear that the method would eventually converge.

configuration	PTM Newton iterations	SSM Newton iterations	relative speed-up of SSM	PTM runtime*	SSM runtime
<i>A</i>	convergence failure	61	–	–	3 sec
<i>B</i>	192,527	51	$> 3775\times$	9 hr 5 min 8 sec	3 sec
<i>C</i>	convergence failure	29	–	–	6 sec
<i>D</i>	convergence failure	46	–	–	14 sec

Table 4: Total Newton’s iterations required to achieve convergence for four configurations of the San Antonio and Guadalupe River network. *The PTM method was terminated after the L2 convergence norm reached 1.6×10^{-4} whereas the SSM was converged to the predefined tolerance of 10^{-6}

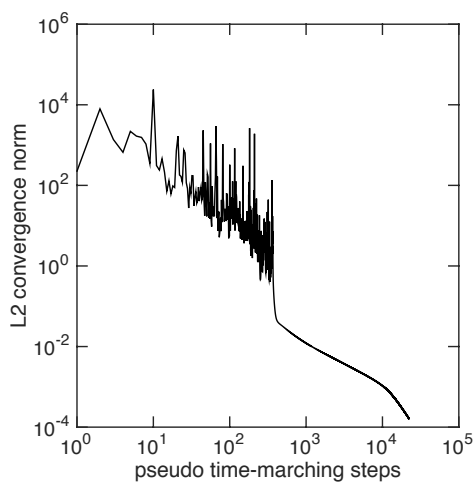


Figure 5: Convergence of the L2 norm between consecutive pseudo-time marching solutions for the PTM with configuration *B* of the San Antonio and Guadalupe River network. Note the above uses the number of time-marching steps as compared to the larger number of Newton iterations provided in Table 4.



5 Discussion

5.1 Model performance

In general, the PTM performed poorly except on very simple systems. As the river network complexity increases the PTM changes from being somewhat slower than SSM to being non-convergent. Indeed, the PTM has only one advantage over the SSM in providing initial conditions to an unsteady SVE solver: specifically, no new code is needed as PTM uses the same unsteady SVE code. However, using PTM for large systems requires a frustrating trial and error approach to tuning the system to obtain convergence. In contrast, the SSM provides a rapid solution to the initial condition problem because Q is computed from simple graph traversal (once through the network), and the subsequent computation of A is “local” (in the sense that in order to correct A , there is no long distance coupling between distant computational nodes). Note that in contrast to PTM, the SSM does not require the modeler to select a set of starting conditions. Thus, different modelers will produce exactly the same $Q(0)$ and $A(0)$ using the SSM on identical geometry, which may not be the case for PTM if modelers must resort to model tuning to obtain convergence.

Herein we only tested two methods for initial conditions, both based on finding the steady-state $\{Q, A\}$ that are consistent with the boundary conditions. However, we can also argue that the cold start and synoptic start (see §1.3) would likely perform as bad or worse than PTM. That the cold start would perform poorly follows from the fact that it has the exact same problem as the PTM (converging over time from inconsistent starting data), but increases the difficulty by trying to converge to the unsteady boundary conditions. A cold start effectively turns the initial condition problem into a spin-up problem. For a cold start model performing similar to the PTM for the San Antonio and Guadalupe River network, we can expect spin-up to require more than 10^4 time-steps of the unsteady solver.

Although a synoptic start might perform better than PTM or a cold start, it seems likely that any approach to interpolating/extrapolating sparse observational data across a larger river network will necessarily result in inconsistencies between the initial $\{Q, A\}$ and the boundary conditions. If such inconsistencies result in model instabilities (a difficult thing to predict), the overall model spin-up time could be extensive. The key problem for the synoptic start is that it requires judgment as to how to best interpolate/extrapolate observational data for initial conditions, which is contrasted to the SSM approach of simply using the actual $Q(0)$ boundary conditions and the steady solver without any further choices by the modeler.



5.2 Effects on spin-up

As alluded to in the Introduction, obtaining an effective model initial condition is only one step in the initialization of an unsteady model. A second step is understanding at what time the model results are independent of any errors or inconsistencies in the initial conditions – i.e. the spin-up time. Some model spin-up time is generally unavoidable as we never have exactly the correct spatially-distributed initial conditions that are exactly consistent with spatially-distributed boundary conditions. In effect, eliminating spin-up time requires a set of initial conditions that are not only consistent with the boundary conditions at $t = 0$, but also consistent with the boundary conditions for $t_m < t < 0$, where t_m represents the system “memory” (or the time interval to wash out a transient impulse).

As an illustration of the scale of the spin-up problem compared to the initial condition problem, we have run the SPRNT unsteady SVE model (Liu and Hodges, 2014) for the San Antonio and Guadalupe River network using 30000+ data points of unsteady lateral inflows for 14 days in January 2010. These boundary condition data were generated from NLDAS. The initial conditions were generated using SSM, as described above. The initial conditions were then perturbed by $\pm 20\%$ in every first-order reach, which provides two slightly inconsistent initial condition data sets to compare to the baseline. In Figure 6, the positive and negative perturbed initial condition cases reach to model equilibrium state (0.001% threshold value) at 152 and 154 hours of simulation time, respectively. Thus, 150 hours represents the time for errors in first-order streams to be diluted in the higher-order (larger) river branches. This can be considered a reasonable estimate of spin-up time for this model of this system given a reasonably consistent set of initial conditions. After 3.8 seconds of CPU time to compute initial conditions using SSM, it only takes an additional 5 minutes of CPU time to complete the spin-up with the SPRNT unsteady model. This is two orders of magnitude faster than the 9+ hours of CPU time required just to compute initial conditions using PTM.

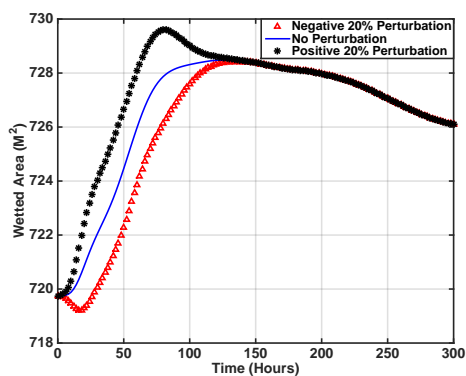


Figure 6: Spin-up for San Antonio and Guadalupe River network with the SPRNT unsteady SVE model initialized using the SSM approach. The positive and negative 20% perturbations are to the Q initial conditions in first-order reaches.



6 Conclusion

Two methods to compute flow (Q) and cross-sectional area (A) initial conditions for an unsteady Saint-Venant river network model have been presented. Both approaches use the steady-state solution for $t = 0$, which provides initial conditions that are smooth and globally consistent with the boundary conditions for the model start time. The Pseudo Time-Marching Method (PTM) is likely similar to undocumented approaches previously used; i.e. application of an unsteady model with constant boundary conditions to achieve a steady solution consistent with initial land surface inflows. For large river networks, the PTM method is slow and inconsistent, arguably depending on the quality of the first guesses for Q and A and the size of the time step required for a stable pseudo-time march. A new Steady-Solution Method (SSM) is developed to address these issues. The SSM computes the initial condition Q in each reach from the inflow boundary conditions of the entire network at $t = 0$ by applying a mass-conservative graph traversal technique. The initial condition A in each reach is found from the solution of the steady-state 1D momentum equation with known Q . The first-guess problem for A is solved as a normal-flow problem with the Chezy-Manning equation and the Q from graph traversal. Although SSM requires writing an additional numerical solver rather than relying on an existing unsteady solver (as used in PTM) our numerical experiments show that SSM is more robust and consistently faster than PTM. Code for both initial condition solvers is publicly available at GitHub (Liu, 2014).

7 Acknowledgements

This material is based upon work supported by the U.S. National Science Foundation under Grant No. CCF-1331610.

8 Notation

A cross-sectional area (m^2)
 b_0 trapezoidal channel bed width (m)
 b_1 trapezoidal channel sidewall slope
 DA drainage Area (mile^2)
 g gravitational acceleration (ms^{-2})
 f generic function
 F equivalent friction geometry ($\text{m}^{-10/3}$)
 h depth (m)
 \bar{n} Manning's roughness ($\text{m}^{-1/3}\text{s}$)



448	P wetted perimeter (m)
449	Q volumetric flow rate (m^3s^{-1})
450	q_l flow rate per unit length through channel sides (m^2s^{-1})
451	r residual function
452	R_h hydraulic radius (m)
453	S_0 channel bottom slope
454	S_f channel friction slope
455	S Strahler order
456	t time (s)
457	W channel width (m)
458	x along-channel spatial coordinate

459 Appendix A: Starting conditions

460 PTM requires starting conditions (or a first guess) of $\{Q(t_0), A(t_0)\}$ for unsteady solution of
 461 eqs. (1) and (2) whereas SSM needs a first guess only for A in the solution of eq. (6). As the
 462 Q solution by the graph traversal method for eq. (5) does not require any starting conditions,
 463 it follows that for the PTM the best choice for $Q(t_0)$ is the same Q developed by simple graph
 464 traversal approach used for SSM (i.e. Alg. 2). To obtain starting conditions for A in SSM or
 465 $A(t_0)$ in PTM, a reasonable guess is the A associated with the “normal depth”, denoted A_n
 466 for the starting Q . The normal depth is obtained from the Chezy-Manning equation solved for
 467 normal flow conditions, i.e.

$$468 Q = \frac{1}{\tilde{n}} A_n R_h^{2/3} S_0^{1/2} \quad (11)$$

469 The hydraulic radius at normal depth requires the area at normal depth and the wetted perimeter
 at normal depth, $R_{h(n)} = A_n/P_n$, which implies Chezy-Manning can be written as:

$$470 A_n = \left(\frac{\tilde{n}Q}{S_0^{1/2}} \right)^{3/5} P_n^{2/5} \quad (12)$$

471 Thus an initial guess for A can be computed for known Q , \tilde{n} , and S_0 , where $P = P(A)$ is a
 472 known piece-wise continuous function based on river bathymetric data. Since $P(A)$ is a nonlinear
 473 function, eq. (12) must be solved with a nonlinear solution method. A simple bi-section method
 can be used following Algorithm 4 with the residual function $r(A)$ defined as:

$$r(A) = \left(\frac{\tilde{n}Q}{S_0^{1/2}} \right)^{3/5} P(A)^{2/5} - A = 0 \quad (13)$$



474 Note that failure to converge for Algorithm 4 is not necessarily fatal; unconverged results are
475 likely to be adequate as they are simply the initial guess for iterative solution by PTM or SSM.
476 As a further simplification, it seems likely that the $P(A)$ in eq. (12) could be approximated
477 using a simple rectangular cross-section, $P(A) = W + 2A/W$, where known channel widths (W)
478 are used. This simplification is valuable in continental-scale river network simulations, where
479 adequate river geometric data throughout a network cannot be guaranteed (Hodges, 2013).

Algorithm 4 Bi-Section Method

```
1: procedure BISECTION( $Q, n, S_0, N_{max}, \epsilon$ ) ▷  $\epsilon$ : tolerance
2:    $A_u \leftarrow 0.01$  ▷ Search for upper bound
3:   repeat
4:      $A_u \leftarrow 2A_u$ 
5:     Evaluate  $r(A)$  in eq. (13)
6:   until  $r > 0$ 
7:    $A_l \leftarrow 0$ 
8:   for  $i = 1$  to  $N_{max}$  do ▷ Bisection method
9:      $r_l \leftarrow r(A_l)$ 
10:     $r_u \leftarrow r(A_u)$ 
11:     $A_m \leftarrow (A_u + A_l)/2$ 
12:    if  $|r_u - r_l| < \epsilon$  then return  $A_m$ 
13:    else
14:       $r_m \leftarrow r(A_m)$ 
15:      if  $r_m > 0$  then
16:         $A_u \leftarrow A_m$ 
17:      else
18:         $A_l \leftarrow A_m$ 
19:      end if
20:    end if
21:  end for
22:  return  $A_m$ 
23: end procedure
```



References

480

481 Abbott, M., Bathurst, J., Cunge, J., O'connell, P., and Rasmussen, J. (1986). An introduction
482 to the european hydrological systemsysteme hydrologique europeen,se, 2: Structure of a
483 physically-based, distributed modelling system. Journal of hydrology, 87(1):61–77.

484 Ajami, H., McCabe, M. F., Evans, J. P., and Stisen, S. (2014). Assessing the impact of model
485 spin-up on surface water-groundwater interactions using an integrated hydrologic model.
486 Water Resources Research, 50(3):2636–2656.

487 Caleffi, V., Valiani, A., and Zanni, A. (2003). Finite volume method for simulating extreme
488 flood events in natural channels. Journal of Hydraulic Research, 41(2):167–177.

489 Chau, K. W. and Lee, J. H. (1991). Mathematical modelling of shing mun river network.
490 Advances in Water Resources, 14(3):106–112.

491 Cormen, T. H., Leiserson, C. E., Rivest, R. L., Stein, C., et al. (2001). Introduction to
492 algorithms, volume 2. MIT press Cambridge.

493 Cunge, J. (1974). Evaluation problem of storm water routing mathematical models. Water
494 Research, 8(12):1083 – 1087.

495 Cunge, J. A., Holly, F. M., and Verwey, A. (1980). Practical aspects of computational river
496 hydraulics.

497 David, C. H., Maidment, D. R., Niu, G.-Y., Yang, Z.-L., Habets, F., and Eijkhout, V. (2011).
498 River network routing on the NHDPlus dataset. Journal of Hydrometeorology, 12:913–934.

499 Hodges, B. R. (2013). Challenges in continental river dynamics. Environmental Modelling &
500 Software, 50:16–20.

501 Hodges, B. R. and Liu, F. (2014). Rivers and electrical networks: Crossing disciplines in
502 modeling and simulation. Foundations and Trends in Electronic Design Automation, 8(1):1–
503 116.

504 Kazolea, M. and Delis, A. (2013). A well-balanced shock-capturing hybrid finite volume–
505 finite difference numerical scheme for extended 1d boussinesq models. Applied Numerical
506 Mathematics, 67:167–186.

507 Kvočka, D., Falconer, R. A., and Bray, M. (2015). Appropriate model use for predicting eleva-
508 tions and inundation extent for extreme flood events. Natural Hazards, 79(3):1791–1808.

509 Lax, P. D. (2006). Gibbs phenomena. Journal of Scientific Computing, 28(2-3):445–449.



- 510 Liang, D., Falconer, R. A., and Lin, B. (2006). Comparison between tvd-maccormack and adi-
511 type solvers of the shallow water equations. Advances in water resources, 29(12):1833–1845.
- 512 Liu, F. (2014). SPRNT: a river dynamics simulator. [https://github.com/frank-y-liu/](https://github.com/frank-y-liu/SPRNT)
513 SPRNT.
- 514 Liu, F. and Hodges, B. R. (2014). Applying microprocessor analysis methods to river network
515 modeling. Environmental Modelling & Software, 52:234–252.
- 516 Nobre, A., Cuartas, L., Hodnett, M., Rennó, C., Rodrigues, G., Silveira, A., Waterloo, M., and
517 Saleska, S. (2011). Height above the nearest drainage – a hydrologically relevant new terrain
518 model. Journal of Hydrology, 404(1–2):13 – 29.
- 519 Ponce, V. M., Simons, D. B., and Li, R.-M. (1978). Applicability of kinematic and diffusion
520 models. Journal of the Hydraulics Division, 104(3):353–360.
- 521 Pramanik, N., Panda, R. K., and Sen, D. (2010). One dimensional hydrodynamic modeling of
522 river flow using dem extracted river cross-sections. Water Resources Management, 24(5):835–
523 852.
- 524 Preissmann, A. (1961). Propagation des intumescences dans les canaux et rivieres. In First
525 Congress French Assoc. for Computation.
- 526 Preissmann, A. and Cunge, J. (1961). Calcul du mascaret sur machine électronique. La Houille
527 Blanche, (5):588–596.
- 528 Rahman, M. M. and Lu, M. (2015). Model spin-up behavior for wet and dry basins: A case
529 study using the xinjiang model. Water, 7(8):4256–4273.
- 530 Rhodes, D. D. (1977). The b-f-m diagram; graphical representation and interpretation of at-a-
531 station hydraulic geometry. American Journal of Science, 277(1):73–96.
- 532 Sanders, B. F. (2001). High-resolution and non-oscillatory solution of the St. Venant equations
533 in non-rectangular and non-prismatic channels. Journal of Hydraulic Research, 39(3):321–330.
- 534 Santibanez, A. R. H. (2015). Evaluating river cross section geometry for a hydraulic river routing
535 model : Guadalupe and San Antonio river basins. Master’s thesis, The University of Texas
536 at Austin, the United State.
- 537 Seck, A., Welty, C., and Maxwell, R. M. (2015). Spin-up behavior and effects of initial conditions
538 for an integrated hydrologic model. Water Resources Research, 51(4):2188–2210.



- 539 Western, A. W., Finlayson, B. L., McMahon, T. A., and O'Neill, I. C. (1997). A method for
540 characterising longitudinal irregularity in river channels. Geomorphology, 21(1):39 – 51.
- 541 Yang, L., Hals, J., and Moan, T. (2012). Comparative study of bond graph models for hydraulic
542 transmission lines with transient flow dynamics. Journal of Dynamic Systems, Measurement,
543 and Control, 134(3):031005.
- 544 Zhao, D., Shen, H., Lai, J., and III, G. T. (1996). Approximate riemann solvers in fvm for 2d
545 hydraulic shock wave modeling. Journal of Hydraulic Engineering, 122(12):692–702.
- 546 Zheng, X. (2016). Texas river hydraulic properties. HydroShare, [http://www.hydroshare.
547 org/resource/40d4dfa1afb04cf9a64831c3419e7443](http://www.hydroshare.org/resource/40d4dfa1afb04cf9a64831c3419e7443).